Journal of Sedimentary Environments (2021) 6:201–212
https://doi.org/10.1007/s43217-021-00051-w

ORIGINAL ARTICLE

Alluvial gold in the Bétaré Oya drainage system, east Cameroon

Kevin Ijunghi Ateh[1] · Cheo Emmanuel Suh[2] · Jeremiah Shuster[3] · Elisha Mutum Shemang[4] · Akumbom Vishiti[5] · Frank Reith[3] · Gordon Southam[6]

Received: 19 November 2020 / Revised: 22 January 2021 / Accepted: 28 January 2021 / Published online: 17 February 2021

Abstract

The morphology and elemental composition of alluvial gold grains from the Bétaré Oya gold district were investigated as part of a district exploration strategy. The morphology and general chemistry of the grains, determined using scanning electron microscopy (SEM)—energy dispersive spectroscopy and electron probe microanalyzer (EMPA), respectively, revealed three categories of grains: (1) gold grains with irregular to regular, bent-up and folded outlines with irregular and pitted surfaces and a flatness index ranging from 2.1 to 4.6; (2) gold grains with regular and polished outlines, smooth surfaces with few or no cavities and a characteristic flatness index range between 3.0 and 8.6; (3) and elongate grains. Rounding of the grains, physical abrasion and bent/folded features suggest that the alluvial gold grains have been transported in a high-energy environment, but not necessarily over long distances from their source rock(s). The gold grains are alloyed with Ag and Cu with concentrations of Ag ranging from 0 to 14.19 wt% whereas Cu concentrations are between 0.03 and 0.15 wt%. SEM images of sites where active weathering of gold is indicated by the presence of colloidal gold, i.e., crevices possessing sedimentary materials on the surface of the grains, revealed the presence of bacteria. All of the gold grains analyzed possess high purity (~ 100% Au) at the water–sediment–gold interface demonstrating that Ag and Cu are highly dispersed in placer systems relative to gold, and that gold can be dissolved and subsequently re-precipitated possibly with the aid of bacteria in alluvial systems.

Keywords Gold · Morphology · Microchemistry · Bacterioform gold

1 Introduction

Placer gold deposits around the world form through the processes of erosion, transportation and deposition of material from gold-rich rocks and/or structures in supergene fluvial environments. Alluvial gold grain morphology, texture and chemistry have been used successfully in the determination of primary gold mineralization type of mineralization and the potential host rock (e.g., Chapman et al. 2009; Moles et al. 2013; Omang et al. 2015; Townley et al. 2003). According to Boyle (1979) Au grains are a natural alloy of Au, Ag, and Cu in proportions that vary with the conditions of ore formation. Various gold types bear characteristic alloy composition and therefore peculiar microchemical signatures. These signatures have been summarized for orogenic gold signatures (Chapman et al. 2000, 2010), epithermal vein signatures (Chapman et al. 2005; Chapman and Mortensen 2006), skarn- and intrusion-related gold signatures (Potter and Styles 2003) and oxidizing chloride hydrothermal systems (Chapman et al. 2009). Recent experimental

Communicated by Mauro Cesar Geraldes.

✉ Kevin Ijunghi Ateh
kevinateh@gmail.com

[1] Department of Mining and Mineral Engineering, The University of Bamenda, North West Region, P.O. Box 39, Bambili, Cameroon

[2] Department of Geology, Mining and Environmental Science, The University of Bamenda, North West Region, P.O. Box 39, Bambili, Cameroon

[3] School of Molecular and Biomedical Science, The University of Adelaide, Adelaide, Australia

[4] Department of Earth and Environmental Sciences, Botswana International University of Science and Technology, Private Bag 16, Palapye, Botswana

[5] Department of Civil Engineering, The University Institute of Technology (IUT), University of Douala, Littoral Region, P.O. Box 8698, Douala, Cameroon

[6] School of Earth and Environmental Sciences, The University of Queensland, Saint Lucia, Australia

works have shown that biogeochemical weathering of gold-bearing ore could be a key phenomenon in the formation of secondary gold deposits. This may be in part due to the action of iron and sulfur oxidizing bacteria and subsequently by sulfate-reducing bacteria that are known to be responsible for the solubilization, precipitation and re-concentration of gold, respectively, under supergene conditions (Lengke et al. 2006a, b, c; Lengke and Southam 2006; Reith et al. 2007; Shuster et al. 2013, 2016; Shuster and Southam 2015).

The link between bacteria and secondary gold precipitation was established in the works of Reith et al. (2006) using scanning electron microscopy (SEM) and confocal scanning laser microscopy (CSLM) combined with nucleic acid staining in which bacterial pseudomorphs and active bacterial biofilms, respectively, were revealed on the surface of these grains. According to Reith et al. (2006) the ability of sulfur oxidizing and reducing bacteria to transform gold complexes into octahedral gold suggests that bacteria contribute to the formation of gold platelets in the supergene environment. Also, Shuster et al. (2016) highlighted the importance of biogeochemical weathering on primary gold-bearing metal sulfide ore which leads to supergene gold enrichment and provide insights on the evolution of the ore deposit over time. According to Shuster and Southam (2015) secondary Au, initially occurring as dispersed nanometer-scale colloids, bacteriomorphic structures, octahedral platelets and micrometer-scale foils continued to develop and aggregate into millimeter-sized grains within sedimentary placer deposits leading to gold grain growth. There is need to back these laboratory results with evidence of secondary gold formation in natural alluvial systems and this is the main thrust of this study.

1.1 Geological setting

The Bétaré Oya alluvial system is located within the Lom Basin which is part of the Central Cameroon Shear Zone (CCSZ), a SW extension of the Central African Shear Zone (CASZ) and constitutes a part of the North Equatorial Central African Fold Belt (NECAFB, Fig. 1a**).** The fold belt is situated at the northern edge of the Congo Craton (Njongfang et al. 2008) and is essentially composed of Palaeoproterozoic basement, traced through Cameroon across the Atlantic into northeastern Brazil and the Trans-Sahara Belt. The CCSZ and its relay feature known as the Sanaga fault (SF) have a NE-SW orientation and is characterized by the abundance of granitic intrusions associated with major shear zones (Ngatcha et al. 2019; Takodjou Wambo et al. 2020). The Lom Basin is composed mainly of metasedimentary rocks, grouped into two main structural and metamorphic units; monocyclic and polycyclic units. The monocyclic unit includes rocks such as volcano-clastic series, orthogneiss, quartzite and polygenic conglomerate (Soba 1989) metamorphosed under greenschist facies and associated with grabens. The polycyclic unit consists of staurolite mica schists, Lom Bridge gneisses, and staurolite-chloritoid mylonites, closely related to the horst structures (Ngako et al. 2003). The mylonites are the key rocks that reveal the presence of the SF (Soba 1989). Quartz veins and granitoids generally intrude both units and show evidence of sinistral deformation.

The Lom basin is characterized by intensive artisanal and semi-mechanized alluvial gold exploitation. Primary gold in the Bétaré Oya district is hosted in quartz veins that truncate meta-sedimentary rocks in the vicinity of small local granitoid intrusions (Vishiti et al. 2017). The quartz veins are thought to be a product of hydrothermal fluids which originated from nearby intrusive bodies. The study area was selected on the basis of the presence of gold in the alluvial system in a granitoid-dominated terrane (Fig. 1c). The area extends from Northing 411,000 to 417,000 and from Easting 626,000 to 633,000, zone 33 N (Fig. 1d). The granitoid intrusion in the study area is sub-alkaline, high K calc-alkaline in nature, granodioritic to tonalitic affinity emplaced in a volcanic arc setting (Ateh et al. 2017). This intrusion is Pan African in age similar to other granitoids along the CCSZ with a mean age of 635 ± 5 Ma (Ateh et al. 2017). The wall rock alteration zone and the vicinity of this Pan African granitoid carries primary gold lodes. It has not also been established whether all the gold within the alluvial deposit is placer or authigenic.

2 Method of study

Stream sediment samples were collected at selected sites shown on Fig. 1d and panned for the heavy mineral concentrate and their visible gold count recorded on site. These samples were later air dried and the gold grains in them picked using binocular microscopes at the Geology Laboratory, University of Buea.

The gold grains were divided into two subsets. The first set was sent to the University of Queensland, Australia where each sample was investigated for its morphology using a scanning electron microscope (SEM) equipped with an energy dispersive spectrometer (EDS). The second set was used to study the chemistry of the grains at Technical University of Clausthal, Germany using electron probe microanalyzer (EMPA). For the EMPA study the detection limits for gold was 5 ppb and 0.1–50 ppm for the Zn, Cu and Ag. Laboratory precision based on replicate analyses was better than 10% at 95% confidence level. The same grains were polished using standard procedure and analyzed using a Cameca SX100 electron microprobe for Ag, As, Au, Ba, Cu, Fe, Pb, S and Zn at the Technical University of Clausthal, Germany. The instrument was

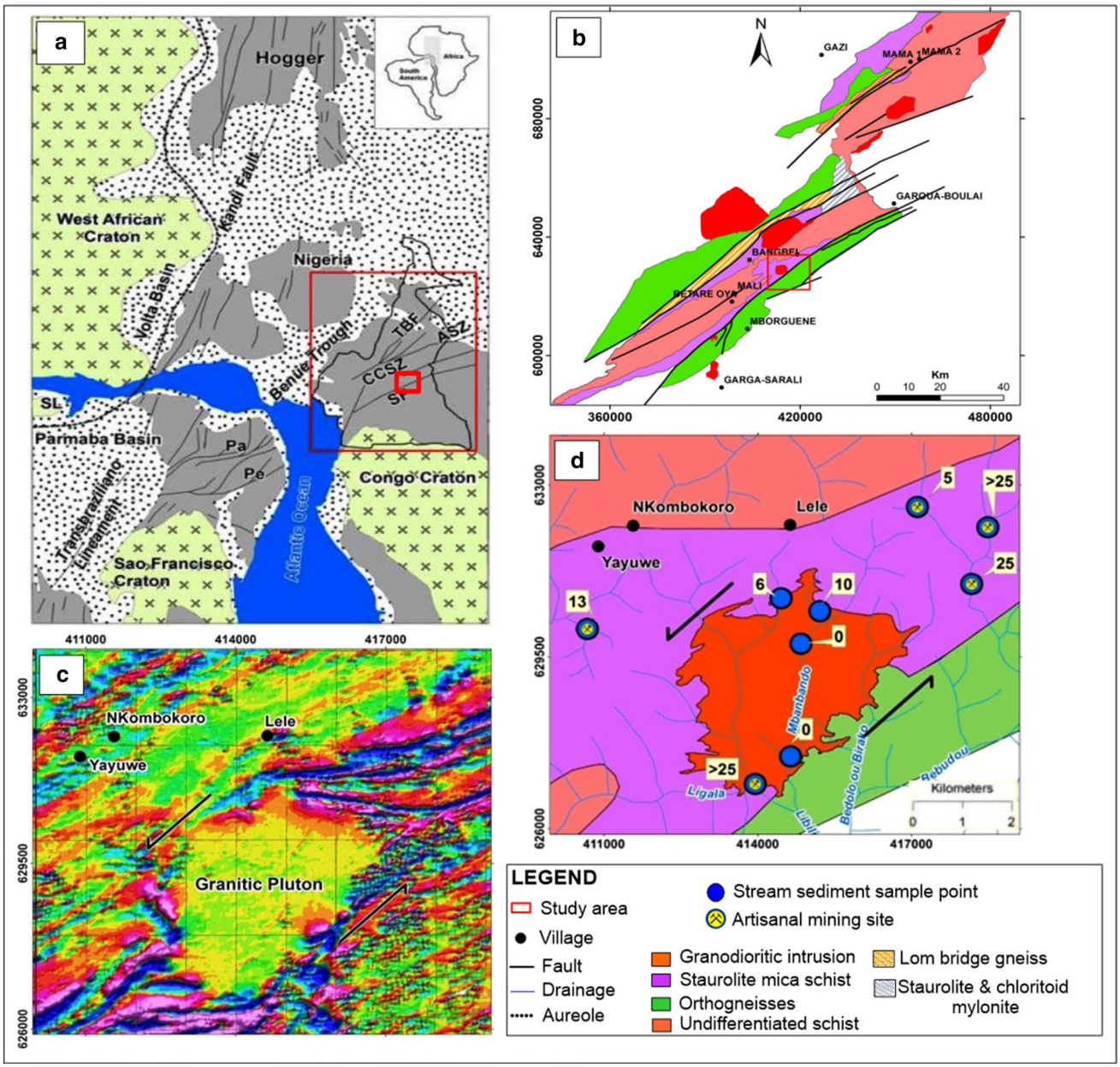

Fig. 1 **a** Regional geologic map situating Cameroon within the central African fold belt (CAFB), **b** location of study area within the lower Lom basin sandwich by the Sanaga fault (SF), **c** aeromagnetic and radiometric survey map of the study area (CAMINCO 2009), **d** stream sediment sample location map. *SF* Sanaga fault, *Pe* Pernambuco Shear Zone, *Pa* Patos Shear Zone, *AS* Adamawa Shear Zone, *TBF* Tcholéré Banyo fault, *CCSZ* Central Cameroon Shear Zone

operated at 20 kV, 40 nA. Pure metals (Ag, Au, Cu, Pd, Se, Pt), pure galena (Pb, S), sphalerite (Zn), HgTe (Hg), GaAs (As), InSb (Sb), cassiterite (Sn), and hematite (Fe), were used as standards. Care was taken to choose analytical points free of cracks. A standard was run after every ten analyses to ensure quality control on the data. The fineness for Au was calculated using the formula (Au*1000)/(Ag + Au) (Hallbauer and Utter 1977).

3 Results

3.1 Gold grain morphology and microtexture

Gold grains from the alluvial system within the Bétaré Oya gold district displayed a variety of shapes and sizes (Fig. 2). Based on morphology, three populations of gold

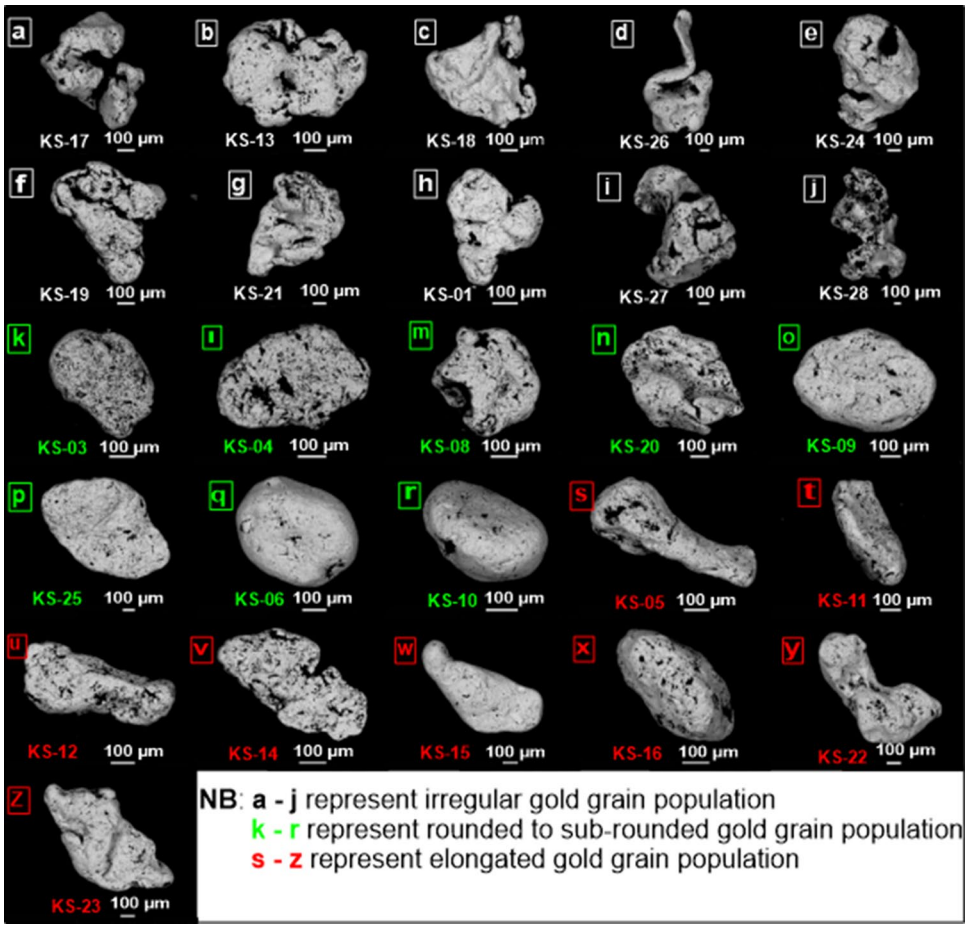

Fig. 2 SEM images of representative gold grains from the Bétaré Oya alluvial system, eastern Cameroon investigated in this study

grains were distinguished. The first group of grains was characterized by irregular shapes and regular edges. Their sizes generally ranged between 350 and 600 µm and can go up to 1 mm (Fig. 2a–j). The second gold grain population was characterized by sub-rounded, rounded, ovoid or spherical grains. These grains were generally pitted although some grains demonstrated smooth surfaces. Grain sizes varied from 400 to ~ 700 µm (Fig. 2k–r). Gold grains from this population were hammered with smooth surfaces. Their outlines were regular showing no clear evidence of primary imprints (Fig. 2n, KS-20). The third gold grain population was characterized as elongated, smooth and/or pitted grains with sizes ranging between 400 and 800 µm.

The SEM study allowed for better appreciation of the surface features of the gold grains (Fig. 3). The microtextures observed on some of the gold grains include cavities, shallow hammer-marks, scratches or furrows, irregular surface pits and abraded embayments up to 20 µm and canals. Most of the cavities were filled with a light gray clayey material and sometimes organic matter. In some cases, dissolution features, often as honey-comb textures were observed (Fig. 3d). Crevices within the gold grains reveal the presence of bacteria and the by-products of their metabolic activities (Fig. 4), i.e., secondary, colloidal and octahedral gold. Bacterial attachment to gold grains was facilitated by exopolymeric substances (Fig. 4b), which also trapped and/or helped form the re-precipitated colloidal gold particles. Surface depressions within the gold grains are extensively covered by bacteria and by bacterioform gold (Fig. 4e, f).

3.2 Gold grain chemistry

Representative EDS spectra of gold grain KS-03 and KS-07 are shown in Fig. 5 while the EMPA data for the grains are presented in Table 1. In addition to Au, other alloy elements include Ag, Cu and Zn. Ag content in the gold grains varied from 0 to 14.19 wt% whereas Cu contents ranged between 0 and 0.15 wt% and Zn in most gold grains was below the detection limit. The concentration of gold in the rims varied from 82.36 to 100.38 wt% and that of the core varied between 83.6 and 100.38 wt%. Gold grain fineness values were calculated and ranged between 859 and 1000. The fineness in the rims varies from 860 to 1000 whereas that of the core ranges from 859 to 1000. On The Au–Cu–Ag plot (Fig. 6) these alluvial gold grains revealed a mesothermal/

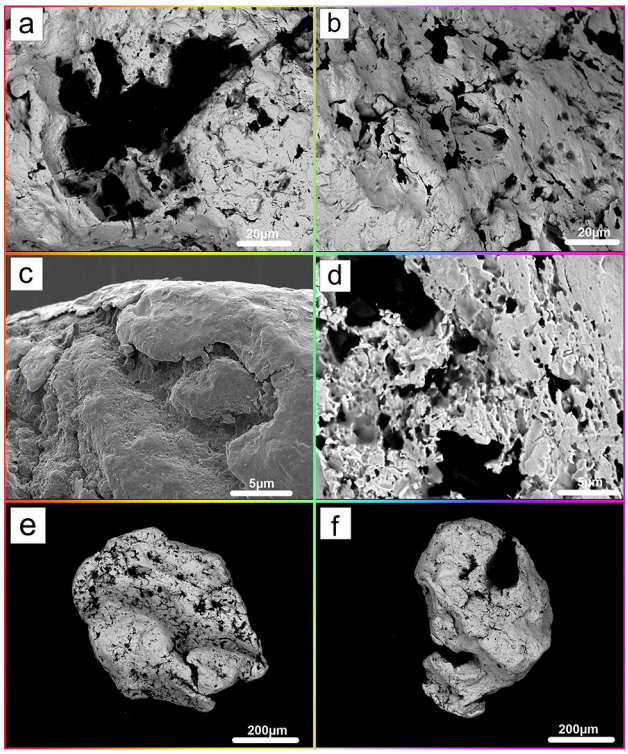

Fig. 3 Microtextures of gold grains from the Bétaré Oya alluvial system **a** cavities, **b** grooves and scratches as a result of abrasion and smearing, **c** embayment and corroded surfaces, **d** dissolution textures and/or cavities, **e** canal and **f** cavity filled with clay/organic matter

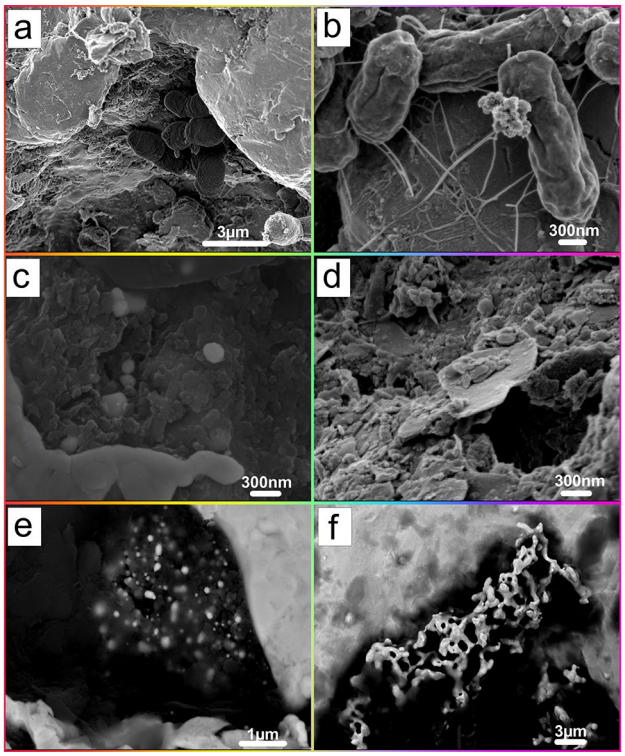

Fig. 4 Microphotographs of gold grain crevices from the Bétaré Oya drainage system. **a** Bacterial colonization, **b** bacterial contact via exopolymer, **c** gold colloids, **d** octahedral gold platelet, **e** secondary gold dispersed in clay-sized materials, **f** network of bacterioform gold on the surface of a gold grain

orogenic origin similar to those reported by Vishiti et al. (2015).

4 Interpretation and Discussion

4.1 Alluvial gold grain morphology and proximity to source rock

The results of this study show that some of the gold grains have irregular morphology and are interpreted to represent newly liberated grains from the source rock. During progressive transformation and separation in stream, the morphology evolves to semispherical, wafer-shaped, and finally flake-shaped. The surface texture of the grains also evolves from smooth and clean to pitted, hackly and, finally to lobate-textured (Groen et al. 1990). These features depend on the stream's energy, sediment type, and composition. Flaky and small size particles are easier to transport; consequently distal placers consist of predominantly flake-shape gold of small size classes. In this study, three main gold populations were distinguished based on shape and outline. The irregular gold grains still preserve outlines, which suggest a relatively short transport distance as compared to the sub-rounded/elongated grains which indicate a moderate distance of transportation. The rounded to oval shaped grains represent long distance of transport. According to Yeend (1975), the features created by hammering and abrasion are recorded by surface texture, related to shape of gold particles showing evolution in response to the changing stream energy and size distribution of host sediments. The microtextures observed within the gold grain population of the Bétaré Oya drainage system such as embayment, scratches and furrows, grooves, etch pits, cavities, corroded surface, honey comb-like textures and canals reveal that the mechanical and corrosion processes are the main processes responsible for their formation. In terms of morphological characterization, Townley et al. (2003) used the shape of placer Au grains to provide a vector to the location of bedrock sources. Based on the physical characteristics of gold particles as outlined by Townley et al. (2003) the gold grains from the Bétaré Oya gold district (BOGD) are potentially derived from two sources.

- Those with irregular to regular, bent-up and folded outlines; irregular and pitted surfaces (cavity full) and an inferred flatness index range between 2.1 and 4.6 which

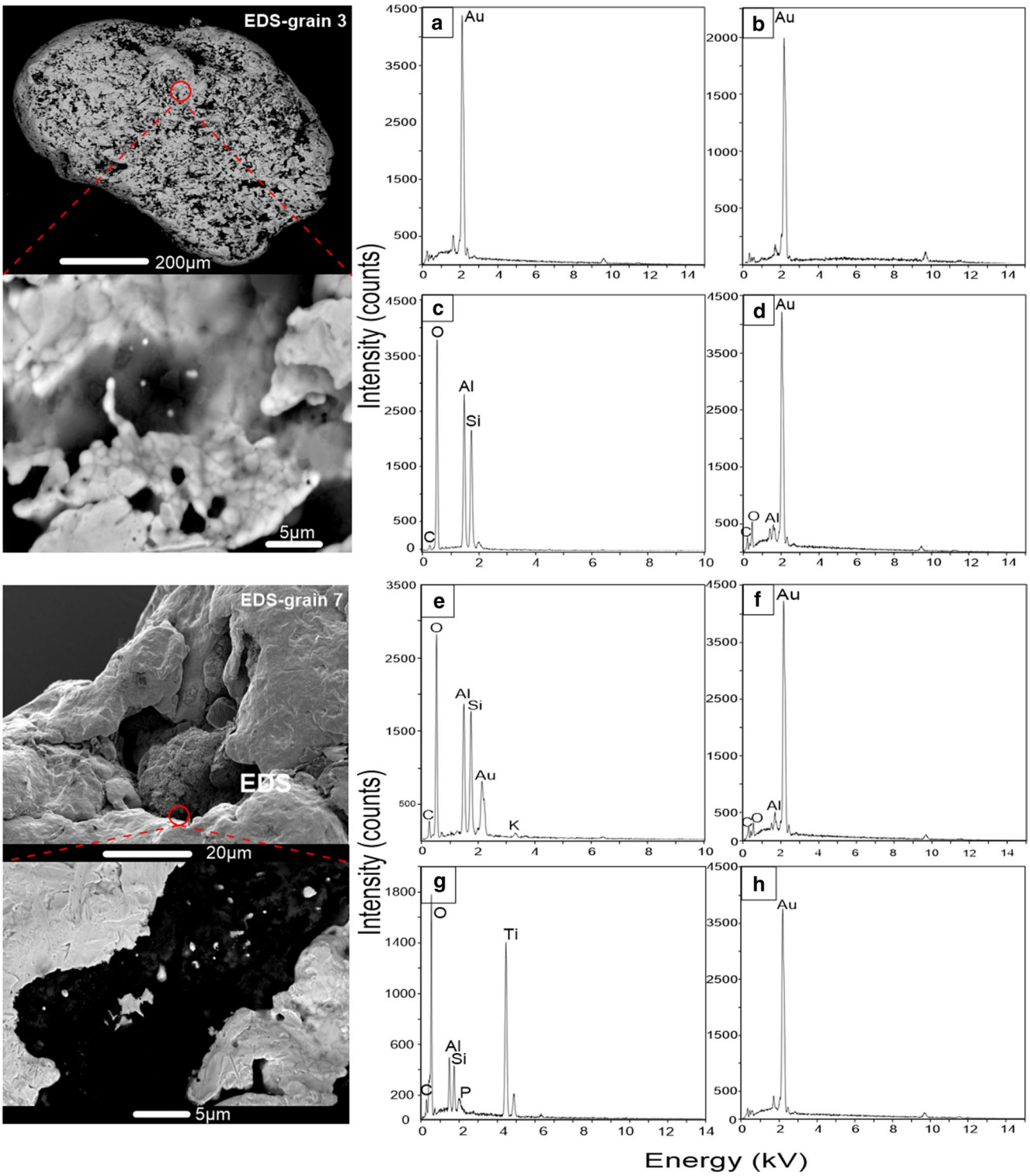

Fig. 5 EDS patterns for gold grain KS-03 and KS-07 investigated in this study

represent gold grains from a source area between 50 and 300 m radius.

- Those with regular and polished outlines, regular topography and little or no cavities on the surfaces and a characteristic flatness index range between 3.0 and 8.6 defining gold grains from a distance to source area within a 300–1000 m radius.

Based on Townley et al. (2003), the proximity to a lode gold source in the Bétaré Oya gold district ranges from 50

Table 1 Ag–Au–Cu–Zn compositional variation of gold grains from the Bétaré Oya gold district

Dataset/point	Gold grains	Position	Ag%	Au%	Cu%	Zn%	Total	Fineness
1/1	Grain 1	Core	12.26	85.35	0.03	0	97.65	877
2/1		Core	12.76	85.99	0.03	0	98.78	873
3/1		Core	12.63	85.84	0.03	0	98.49	874
4/1		Core	12.57	86.1	0.02	0	98.69	875
5/1		Core	12.28	87.22	0.02	0	99.52	878
6/1		Core	12.7	86.4	0.02	0	99.12	873
7/1		Core	0.91	96.87	0.01	0	97.79	991
8/1		Core	5.02	95.88	0.01	0	100.91	950
9/1		Rim	4.08	93.54	0.02	0	97.63	959
10/1		Rim	0.63	92.93	0	0	93.56	994
11/1		Core	1.66	99.37	0	0	101.03	983
12/1		Core	1.41	97.53	0	0	98.95	986
13/1	Grain 2	Rim	6.6	15.52	0.11	0.04	22.27	913
14/1		Rim	0	33.38	0	0	33.38	1000
15/1		Rim	1.11	97.03	0	0	98.14	989
16/1		Rim	12.66	85.33	0.01	0	98	874
17/1		Rim	2.03	94.92	0	0	96.96	980
18/1		Rim	7.71	54.31	0	0	62.02	919
19/1		Core	13.76	83.85	0	0	97.61	862
20/1		Core	13.78	83.6	0	0	97.38	862
21/1		Core	13.64	83.78	0	0	97.42	864
22/1		Core	13.62	83.67	0	0	97.29	864
23/1		Core	13.75	84.85	0.01	0	98.61	863
37/1	Grain 5	Rim	0.53	98.57	0	0	99.1	995
38/1		Rim	0.52	87.88	0.15	0	88.55	995
39/1		Core	0.47	97.59	0	0	98.05	995
40/1		Core	0.86	96.92	0	0	97.79	991
41/1		Core	0.82	96.86	0	0	97.68	992
42/1		Rim	1.15	96.86	0	0	98.01	989
43/1		Core	1.35	98.03	0	0	99.38	987
44/1		Core	13.01	85.57	0.02	0	98.6	870
45/1		Core	12.89	85.81	0.01	0	98.71	871
46/1		Core	12.75	85.12	0.02	0	97.89	873
47/1		Core	12.98	85.22	0.01	0	98.21	870
48/1		Core	12.92	85.31	0.02	0	98.25	871
49/1		Core	13.28	84.5	0.01	0	97.79	867
50/1		Core	12.76	84.93	0.02	0	97.71	872

Table 1 (continued)

Dataset/point	Gold grains	Position	Ag%	Au%	Cu%	Zn%	Total	Fineness
17/1	Grain 7	Core	13.78	87	0.01	0	100.78	864
18/1		Core	13.82	86.78	0	0	100.6	862
19/1		Core	13.4	87.28	0.01	0	100.69	867
20/1		Core	13.88	86.65	0.01	0	100.54	862
21/1		Core	14.03	86.75	0.01	0	100.79	860
22/1		Core	13.8	86.85	0.02	0	100.66	863
23/1		Core	13.24	86.19	0.01	0	99.43	868
24/1		Rim	14.19	87.21	0.01	0	101.41	859
25/1		Rim	14.03	86.45	0.01	0	100.49	860
26/1		Rim	0.3	99.83	0	0	100.14	997
27/1		Rim	3.53	96.23	0	0	99.76	965
28/1		Core	0.68	99.75	0	0	100.43	993
29/1		Core	2.2	97.44	0	0	99.64	978
30/1		Core	0.64	99.21	0	0	99.85	994
31/1		Core	0.26	98.15	0	0	98.41	997
32/1		Core	0.69	98.89	0	0	99.58	993
24/1	Grain 8	Core	14.03	86.49	0.02	0	100.53	860
25/1		Core	14.01	86.64	0.02	0	100.67	861
26/1		Core	13.86	86.44	0.01	0	100.32	862
27/1		Core	13.89	87.24	0.02	0	101.15	862
28/1		Core	13.96	86.98	0.02	0	100.96	861
29/1		Core	13.96	87.4	0.02	0	101.38	861
30/1		Core	13.64	87.29	0.01	0	100.94	864
31/1		Core	0.36	100.38	0	0	100.74	996
32/1		Core	0.14	100.31	0	0	100.44	999
33/1		Core	0.93	99.41	0	0	100.33	991
34/1		Core	0.18	99.61	0	0	99.8	998
35/1		Rim	0.03	82.36	0	0	82.39	1000
36/1		Rim	0.22	100.31	0	0	100.52	998
1/1	Grain 9	Core	2.8	96.85	0	0	99.66	972
2/1		Core	3.69	96.47	0	0	100.17	963
3/1		Core	6.09	93.72	0	0	99.81	939
4/1		Core	3.59	96.91	0	0	100.51	964
5/1		Core	9.49	89.97	0.01	0	99.47	905
6/1		Core	0.8	98.79	0.01	0	99.6	992
7/1		Rim	12.66	85.83	0	0	98.5	874
8/1		Rim	2.22	98.14	0	0	100.37	978
9/1		Rim	7.62	92.32	0.02	0	99.97	924
10/1		Rim	12.73	86.61	0	0	99.35	873
11/1		Core	12.77	85.87	0.01	0	98.65	873
12/1		Core	12.65	86.13	0.01	0	98.78	874
13/1		Core	12.57	85.79	0.01	0	98.36	875
14/1		Core	12.81	85.79	0	0	98.61	872
15/1		Core	13.21	85.68	0.01	0	98.89	868
16/1		Core	12.74	85.42	0.01	0	98.17	873

Table 1 (continued)

Dataset/point	Gold grains	Position	Ag%	Au%	Cu%	Zn%	Total	Fineness
51/1	Grain 11	Core	13.87	86.14	0.02	0	100.03	862
52/1		Core	12.46	86.17	0.02	0	98.65	876
53/1		Core	13.37	84.98	0.02	0	98.36	866
54/1		Core	12.98	86.42	0.02	0	99.41	871
55/1		Core	13.09	85.8	0.01	0	98.9	869
56/1		Core	13.41	86.33	0.02	0	99.76	866
57/1		Core	13.51	86.3	0.02	0	99.83	865
58/1		Rim	13.64	86.32	0.02	0	99.98	864
59/1		Rim	1.2	97.81	0.01	0	99.02	988
60/1		Rim	0.57	86.09	0.02	0	86.69	994
61/1		Core	0.34	97.25	0	0	97.6	997
62/1		Core	2.22	96.1	0	0	98.32	978
63/1		Core	0.74	96.6	0	0	97.34	993
64/1		Core	0.41	97.77	0	0	98.18	996
65/1		Core	0.39	97.42	0	0	97.81	996
33/1	Grain 12	Core	13.44	86.34	0.02	0	99.8	866
34/1		Core	13.03	86.38	0.03	0	99.43	870
35/1		Core	13.18	86.55	0.03	0	99.76	869
36/1		Core	13.21	86.53	0.03	0	99.77	868
37/1		Core	13.42	85.98	0.03	0	99.44	866
38/1		Core	13.41	86.36	0.03	0	99.8	866
39/1		Core	13.4	86.22	0.02	0	99.64	866
40/1		Rim	13.25	85.83	0.03	0	99.1	868
41/1		Rim	13.41	86.11	0.03	0	99.54	866
42/1		Rim	0.26	99.12	0	0	99.39	997
43/1		Rim	2.19	96.48	0	0	98.67	978
44/1		Core	0.58	99.07	0	0	99.65	994
45/1		Core	0.01	98.91	0	0	98.92	1000
46/1		Core	0.2	98.84	0	0	99.03	998
47/1		Core	0.61	98.62	0	0	99.24	994
48/1		Core	0.41	98.92	0	0	99.33	996
49/1		Core	0.26	98.67	0	0	98.93	997
50/1		Core	0.34	98.16	0	0	98.5	997
51/1	Grain 21	Core	13.33	87.41	0.01	0	100.75	867
52/1		Core	13.34	86.88	0.01	0	100.23	867
53/1		Core	13.35	87.03	0.01	0	100.39	867
54/1		Core	13.43	87.41	0.01	0	100.85	866
55/1		Core	13.43	87.89	0.01	0	101.34	866
56/1		Core	13.38	87.07	0.02	0	100.47	867
57/1		Core	1.41	99.2	0	0	100.6	986
58/1		Core	0.19	97.89	0.02	0	98.1	998
59/1		Core	0.53	99.22	0	0	99.75	995
60/1		Core	0.19	99.13	0	0	99.32	998
61/1		Core	0.97	97.62	0	0	98.59	990
62/1		Rim	0.14	90.95	0	0	91.1	999

to 1000 m up-gradient from these sample sites. This distance corresponds to a proximal primary gold mineralized zone characterized by the presence of wall rock alteration such as seritization, silicification and albitization (Vishiti

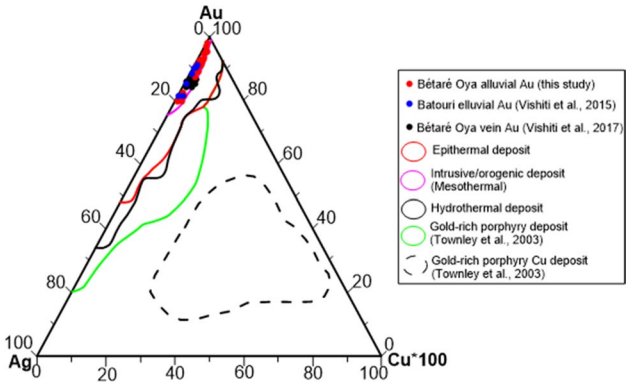

Fig. 6 Ternary Au–Cu–Ag plots of the compositions of Au grains from the Bétaré Oya gold district compared with those from the Kazikkaya—Turkey lode gold, Hunker dome lode, Grasberg, Indonesia, Santo Tomas II, Philippines, and Cerro Casale gold porphyry northern Chile. The Bétaré Oya gold grain samples show mesothermal, orogenic/or intrusion-related signature

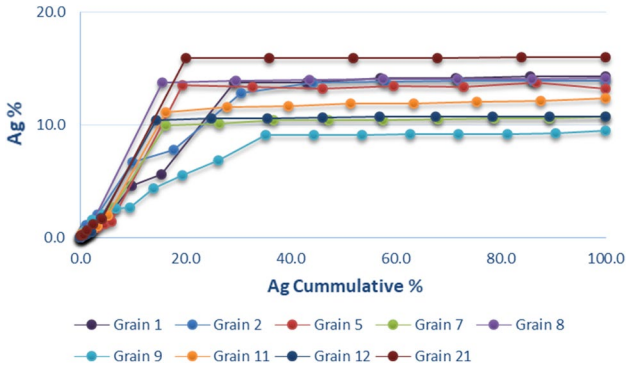

Fig. 7 Ag content variation of alluvial gold grain populations from the drainage system investigated in this study area, highlighting the enrichment of pure gold at the gold grains surfaces

et al. 2017) in the vicinity of the local granodioritic intrusion (Ateh et al. 2017) in the Bétaré Oya gold district.

4.2 Lode gold proximity in relation to microchemical signature of alluvial gold

Morphological characterization and microchemical signature of alluvial gold grains have been used to establish a correlation between the gold grains from bedrock and alluvial populations (Youngson et al. 2002). According to Chapman et al. (2000) the degree of agreement between the microchemical signatures of bedrock and associated alluvial gold is influenced by the geomorphological development of the locality. In the cases where gold-bearing structures are being actively eroded by rivers, the degree of correlation between the characteristics of the bedrock and alluvial gold populations is very high. The abundance of alluvial gold within the drainage system is influenced by the orientation of the mineralization in relation to the river valley, particularly where the intersection is either parallel or perpendicular to the mineralized structure (Chapman et al. 2000). With the mineralization structure lying along the river valley contributing more gold into the stream sediments than when it cuts across. According to Chapman et al. (2000) 'rough' grains, with attached quartz particles, are likely to have experienced a smaller degree of fluvial transport than the corresponding 'smooth' grains, and are probably derived from more local sources. This hypothesis is supported by the variation in silver content in alluvial gold grains (Chapman et al. 2010 Chapman et al., 2011; Morrison et al.,1991; Nakagawa et al., 2005; Nesterenko et al., 2014). Alluvial gold grains that have traveled short distances from their lode sources are generally rough with little or no variation in its Ag content. Alluvial gold grains from the Bétaré Oya gold district reveal rough edges associated with an almost flatten curve in the Ag % vs Ag cumulative plot (Fig. 7). This plot reveals an almost uniform Ag concentration in the gold grains. The Ag content alongside the gold grain morphology support a close proximity to the lode source in the Bétaré Oya gold district.

4.3 Evidence of secondary gold deposit resulting from weathering of primary ore and microbial activity in the BOGD

Primary gold grains from mineralized quartz veins in the Bétaré Oya gold district were investigated for their chemistry and it revealed a microchemical signature of Au + Ag ± Cu ± Hg ± Se (Vishiti et al. 2018). Alluvial gold from creeks draining the Bétaré Oya gold district were analyzed and revealed a similar microchemical signature Au + Ag ± Cu. The similarity in the gold chemistry suggest that alluvial gold is a direct consequence of weathering of mineralized veins by streams that drain the gold district. Gold grains from the creeks of Bétaré Oya reveal Au-rich rims and Ag rich cores. This is explained by the continuous leaching of Ag and Au, combined with the re-precipitation of Au during gold grain transport thereby improving upon gold fineness (purity).

SEM images of gold crevices for gold grains from the Bétaré Oya gold district reveal the existence of bacteria on these gold grains. According to Reith et al. (2007) gold-associated bacteria are capable of actively catalyzing the reductive precipitation of toxic gold (I/III) complexes, which improves their survival in such environments. Supergene gold enrichment processes and the mobility of gold have been attributed to thiosulphate and chloride ions—two ligands able to form soluble gold complexes depending on the geochemistry of the environment (Boyle 1979). However, according to Lengke and Southam (2006) these soluble gold complexes are destabilized in the presence of chemolithotrophic bacteria such as iron and sulfur—oxidizing

bacteria and sulfate-reducing bacteria. These bacteria can act as reducing agent, leading to the formation of elemental gold colloids. SEM micrographs of the Bétaré Oya alluvial gold reveals textural evidence of bioaccumulation of secondary gold precipitates, potentially as a result of microbial activity. These images show the presence of bacteria held together by extracellular polymeric substances which trap precipitated octahedral and colloidal gold. Biogeochemical weathering on primary bearing metal sulfide ore is known to lead to supergene gold enrichment and hence provide insight on the evolution of ore deposits over time (Shuster et al. 2016). The presence of bacteria in the vicinity of lode gold mineralization in the BOGD is suggestive of a potential host of economical supergene gold enrichment. This gold is said to be authigenic as it is formed from in situ biogeochemical processes and different from the processes that led to the formation of the lode gold. Shuster and Southam (2015) investigated and established gold grain growth through the agglomeration of nanophase gold particles to micrometer size and subsequently to mm-scale nuggets. This agglomeration of nanophase gold particles is evident in SEM images of the crevices of gold grains from the BOGD. EDS peaks from re-precipitated gold via biogeochemical weathering possess high Au fineness.

5 Conclusion

Based on shape and microtextures of gold grains recovered from alluvial deposits within the Bétaré Oya gold district, the gold is sourced from a proximal lode gold deposit, i.e., within 1 km. Gold grains from the Bétaré Oya drainage system are generally alloyed with Ag and Cu. However, some small grains have high purity, ~ 100% Au suggesting they are entirely secondary. Many grains reveal rough edges with little or no variation in Ag content. The Ag content alongside the gold grain morphology support a close proximity to the lode source in the Bétaré Oya gold district. SEM images reveal the presence of bacteria that likely contributed to the solubilization, re-precipitation and concentration of high purity gold (authigenic gold) in the supergene environment of Bétaré Oya.

Acknowledgements This paper acknowledges the contributions from Prof. Lehmann for generating the chemistry of the gold grains at the Technical University of Clausthal, Germany. This manuscript benefited significantly from comprehensive comments by an anonymous reviewer.

Author contributions KIA carried out the field study, sample collection and processing and, initiated and wrote the first draft of the manuscript. CES designed the project in cooperation with KIA and guided the analytical procedures for all the samples and reviewed, read and approved the manuscript. JS, FR and GS analyzed the gold grains using the SEM in Australia, provided data interpretation insights, read, corrected and approved the manuscript. VA and EMS assisted in the acquisition and interpretation of the EMPA data and read, contributed to and approved the manuscript.

Funding CES and KIA acknowledge support from the Alexander von Humboldt Foundation for the analytical work at TU Clausthal with the support of Prof. Dr. Bernd Lehmann.

Data availability All data used in this study will be readily available to the public.

Compliance with ethical standards

Conflict of interest The authors declare that they have no conflict of interest.

References

Ateh, K. I., Suh, C. E., Shemang, E. M., Vishiti, A., Tata, E., & Chombong, N. N. (2017). New LA-ICP-MS U-Pb ages, Lu-Hf systematics and REE characterization of zircons from a granitic pluton in the Bétaré Oya gold district, SE Cameroon. *Journal of Geoscience and Geomatics, 5,* 267–283.

Boyle, R.W. (1979). *The geochemistry of gold and its deposits* (p. 280). Geological Survey of Canada.

CAMINCO - Cameroon Mining Cooperation is not a reference but the company who carried out the aeromagnetic survey in 2009

Chapman, R. J., Leake, R. C., Bond, D. P. G., Stedra, V., & Fairgrieve, B. (2009). Chemical and mineralogical signatures of gold formed in oxidizing chloride hydrothermal systems and their significance within populations of placer gold grains collected during reconnaissance. *Economic Geology, 104,* 563–585.

Chapman, R. J., Leake, R. C., & Moles, N. R. (2000). The use of microchemical analysis of alluvial gold grains in mineral exploration: experiences in Britain and Ireland. *Journal of Geochemical Exploration, 71,* 241–268.

Chapman, R. J., & Mortensen, J. K. (2006). Application of microchemical characterization of placer gold grains to exploration for epithermal gold mineralization in regions of poor exposure. *Journal of Geochemical Exploration, 91,* 1–26.

Chapman, R. J., Mortensen, J. K., Crawford, E., & Lebarge, W. (2010). Microchemical studies of placer and lode gold in Bonanza and Eldorado creeks, Klondike District, Yukon, Canada: evidence for a small, gold-rich, orogenic hydrothermal system. *Economic Geology, 105,* 1393–1410.

Chapman, R. J., Mortensen, J. K., & Lebarge, W. (2011). Styles of lode gold mineralization contributing to the placers of the Indian River and Black Hills Creek, Yukon Territory, Canada as deduced from microchemical characterization of placer gold grains. *Mineralium Deposita, 46,* 881–903.

Chapman, R. J., Shaw, M. H., Leake, R. C., & Jackson, B. (2005). Gold in the Central Ochil Hills, Scotland. *Applied Earth Science, 114,* 53–64.

Groen, J. C., Craig, J. R., & Rimstidt, J. D. (1990). Gold-rich rim formation on electrum grains in placers. *Canadian Mineralogist, 28,* 207–228.

Hallbauer, D. K., & Utter, T. (1977). Geochemical and morphological characteristics of gold particles from recent river deposits and the fossil placer of the Witwatersrand. *Mineralium Deposita, 12,* 293–306.

Lengke, M. F., Fleet, M. E., & Southam, G. (2006a). Morphology of gold nanoparticles synthesized by filamentous cyano-bacteria from gold (I)-thiosulfate and gold (III)-chloride complexes. *Langmuir, 22,* 2780–2787.

Lengke, M. F., Fleet, M. E., & Southam, G. (2006b). Bioaccumulation of gold by filamentous cyanobacteria between 25 and 200°C. *Geomicrobiology Journal, 23,* 591–597.

Lengke, M. F., Ravel, B., Fleet, M. E., Wanger, G., Gordon, R. A., & Southam, G. (2006c). Mechanisms of gold bio-accumulation by filamentous cyanobacteria from gold (III)-chloride complex. *Environmental Science and Technology, 40,* 6304–6309.

Lengke, M., & Southam, G. (2006). Bioaccumulation of gold by sulfate-reducing bacteria cultured in the presence of gold (I)-thiosulfate complex. *Geochimica et Cosmochimica Acta, 70,* 3646–3661.

Moles, N. R., Chapman, R. J., & Warner, R. B. (2013). Hydrothermal systems reconnaissance exploration and understanding gold-depositing. *Geochemistry: Exploration, Environment, Analysis, 13,* 67–85.

Morrison, G. W., Rose, W. J., & Jaireth, S. (1991). Geological and geochemical controls on the silver content (fineness) of gold in gold–silver deposits. *Ore Geology Reviews, 6,* 333–364.

Nakagawa, M., Santoshl, M., Nambiar, C. G., & Matsubaral, C. (2005). Morphology and chemistry of placer gold from Attappadi Valley, southern India. *Gondwana Research, 8,* 213–222.

Nesterenko, G. V., Roslyakov, N. A., Zhmodik, S. M., Kalinin, Y. A., Morozova, N. S., Kirillov, M. V., & Osintsev, S. R. (2014). Character of gold mineralization in the Late Cenozoic alluvium of the Bauntov area (Vitim highland, Transbaikal region). *Lithology and Mineral Resources, 49,* 29–46.

Ngako, V., Affaton, P., Nnange, J.M., & Njanko, J.T. (2003). Pan-African tectonic evolution in central and southern Cameroon: transpression and transtension during sinistral shear movements. *Journal of African Earth Sciences, 36,* 207–214.

Ngatcha, R. B., Okunlola, O. A., Suh, C. E., Ateh, K. I., & Hofmann, A. (2019). Petrochemical characterization of Neoproterozoic Colomine granitoids, SE Cameroon: implications for gold mineralization. *Lithos, 344–345,* 175–192.

Njongfang, E., Ngako, V., Moreau, C., Affaton, P., & Diot, H. (2008) Restraining bends in high temperature shear zones: the "Central Cameroon Shear Zone", Central Africa. *Journal of African Earth Sciences, 52,* 9–20.

Omang, B. O., Suh, C.E., Lehmann, B., Vishiti A., Chombong, N.N., Fon, A.N., Egbe, J.A., Shemang, E.M. (2015). Microchemical signatures of alluvial gold from two contrasting terrains in Cameroon. *Journal of African earth Sciences 112,* 1–14.

Potter, M., & Styles, M. T. (2003). Gold characterization as a guide to bedrock sources for the Estero Hondo alluvial gold mine, western Ecuador. *Transactions of the Institution of Mining and Metallurgy, Section B: Applied Earth Sciences, 112,* 297–304.

Reith, F., Lengke, M. F., Falconer, D., Craw, D., & Southam, G. (2007). The geomicrobiology of gold. *International Society for Microbial Ecology (ISME), 1,* 567–584.

Reith, F., Rogers, S. L., McPhail, D. C., & Webb, D. (2006). Biomineralization of gold: biofilms on bacterioform gold. *Science, 313,* 333–336.

Soba, D. (1989). La série du Lom: etude géologique et géochronologique d'un bassin volcanosédimentaire de la chaîne panafricaine à l'Est Cameroun. Thèse de Doctorat d'Etat, Université De Paris VI, 181p.

Shuster, J., Lengke, M., Márquez-Zavalía, M. F., & Southam, G. (2016). Floating gold grains and nanophase particles produced from the biogeochemical weathering of a gold-bearing ore. *Economic Geology, 111,* 1485–1494.

Shuster, J., Marsden, S., Maclean, L.C.W., Ball, J., Bolin, T., & Southam, G. (2013). The immobilization of gold (III) chloride by a halophilic sulphate reducing bacterial consortium. In G.R.T. Jenkin (Ed.), *Ore deposits in an evolving Earth* (p. 393). Geological Society of London Special Publication.

Shuster, J., & Southam, G. (2015). The in vitro "growth" of gold grains. *Geology, 48,* 79–82.

Suh, C. E., & Lehmann, B. (2003). Morphology and electron-probe microanalysis of residual gold-grains at Dimako, Southeast Cameroon. *Neues Jahrbuch Für Mineralogie - Monatshefte, 6,* 255–275.

Takodjou Wambo, J. D., Beiranvand, A. P., Ganno, S., Asimow, D. P., Zoheir, B., Salles, R., et al. (2020). Identifying high potential zones of gold mineralization in a sub-tropical region using Landsat-8 and ASTER remote sensing data: a case study of the Ngoura-Colomines goldfield, Eastern Cameroon. *Ore Geology Reviews, 122,* 103530.

Townley, B. K., Hérail, G., Maksaev, V., Palacios, C., De Parseval, P., Sepulveda, F., et al. (2003). Gold grain morphology and composition as an exploration tool: application to gold exploration in covered areas. *Geochemistry: Exploration, Environment, Analysis, 3,* 29–38.

Vishiti, A., Suh, C. E., Lehmann, B., Egbe, J. A., & Shemang, E. M. (2015). Gold grade variation and particle microchemistry in exploration pits of the Batouri gold district, SE Cameroon. *Journal of African Earth Sciences, 111,* 1–13.

Vishiti, A., Suh, C.E., Lehmann, B., Shemang, E.M., Ngome, N.L.J. Nshanji, J.N., Chinjo, F.E., Mongwe, O.Y., Egbe, A.J., and Petersen, S., (2017). Mineral chemistry, bulk rock geochemistry, and S-isotope signature of lode-gold mineralization in the Bétaré Oya gold district, south-east Cameroon. Geological Journal. https://doi.org/10.1002/gj.3093.

Vishiti, A., Suh, E. C., Lehmann, B., Shemang, E. M., Ngome, N. L., Nshanji, N. J., et al. (2018). Mineral chemistry, bulk rock geochemistry, and S-isotope signature of lode-gold mineralization in the Bétaré Oya gold district, south-east Cameroon. *Geological Journal, 53,* 2579–2596.

Yeend, W. (1975). Experimental abrasion of detrital gold. *US Geological Survey Journal of Research, 3,* 203–212.

Youngson, J. H., Woperies, P., Kerr, L. C., & Craw, D. (2002). Au-Ag-Hg and Au-Ag alloys in Nokomai and Nevis valley placers, northern Southland, and Central Otago, New Zealand, and implications for placer-source relationships. *New Zealand Journal of Geology and Geophysics, 45,* 53–69.